

**A 481pJ/decision 3.4M decision/s Multifunctional Deep In-memory Inference Processor  
using Standard 6T SRAM Array**

Mingu Kang, Sujan Gonugondla, Ameya Patil, and Naresh Shanbhag

Dept. Electrical and Computer Engineering, University of Illinois at Urbana-Champaign

**Abstract**

This paper describes a multi-functional deep in-memory processor for inference applications. Deep in-memory processing is achieved by embedding pitch-matched low-SNR analog processing into a standard 6T 16KB SRAM array in 65 nm CMOS. Four applications are demonstrated. The prototype achieves up to 5.6X (9.7X estimated for multi-bank scenario) energy savings with negligible ( $\leq 1\%$ ) accuracy degradation in all four applications as compared to the conventional architecture.

Emerging inference applications require processing of huge data volumes [1]. A conventional inference architecture (Fig. 1) implements memory access, data transfer from memory to processor, data aggregation, and slicing. In such architectures, memory access energy dominates, e.g., an 8-b SRAM read access and an 8-b MAC consumes 5pJ and 1pJ in 65nm CMOS, respectively. Additionally, the memory-processor interface presents a severe throughput bottleneck. Deep in-memory signal processing concept was proposed in [2] to overcome these challenges by embedding mixed-signal processing in the periphery of the SRAM bit-cell array (*BCA*). However, an IC implementation needs to address a host of new challenges including the stringent row & column pitch-matching requirements imposed by the *BCA* without altering its storage density or its read/write functionality, and enabling multiple functions with mixed signal circuitry. Recently [3], a single function, 5×1-b in-memory classifier IC has been demonstrated.

The proposed deep in-memory inference architecture has four stages (Fig.1): 1) multi-row functional read (*MR-FR*), 2) bit-line (*BL*) processing (*BLP*), 3) cross *BL* processing (*CBLP*), and 4) ADC and slicing. The *MR-FR* accesses multiple rows in one pre-charge cycle using pulse-width modulated word-line (*PWM-WL*) signals to generate a *BL* voltage drop proportional to a weighted sum of multiple bits stored in multiple rows in the column, and also performs word-level add/subtract. The *BLP* implements reconfigurable column pitch-matched mixed-signal circuits to execute computations such as multiply/absolute value/comparison on the *BL* voltages, in a massively column-parallel fashion. The *CBLP* aggregates the *BLP* outputs into a scalar which is sliced to obtain the final decision. The *BLP* and *CBLP* can be reconfigured to operate the architecture in either a dot product (*DP*) mode or Manhattan distance (*MD*) mode. Reconfigurable stages enable multiple functions (Fig. 1 table) including normal read/write.

The chip architecture (Fig. 2) includes a digital controller (CTRL) and a CORE. The normal

read/write circuitry (lower) and in-memory processing blocks (upper) are physically separated to maintain functionality. Functional  $WL$  drivers generate  $PWM-WL$  signals while the reconfiguration word ( $RCFG$ ) reconfigures local controllers in the CTRL. The in-memory processing chain is pipelined to enable  $BL$  pre-charge when the  $MR-FR$  step is complete. The architecture processes 128 8-b words per access cycle requiring two consecutive access cycles to process a 256-dimensional vector with 8-b elements. Thus, two consecutive  $CBLP$  outputs are sampled on different sampling capacitors and charge-shared before conversion by the ADC. Four 8-bit single-slope slow but energy efficient ADCs execute in parallel to process 36 128-dimensional vectors/ $\mu$ s.

The  $MR-FR$  step (Fig. 3) generates  $BL$  swing  $\Delta V_{BL}$  proportional to binary-weighted bits ( $d_i$ ) in a column [2] via the use of  $PWM-WL$  signals. An 8-b array data ( $D$ ) and streamed input ( $P$ ) precision is chosen to satisfy the requirements of many inference applications. The longest  $PWM-WL$  pulse width with  $V_{WL} < V_{DD}$  is chosen to be less than 40% of  $BL$  RC time constant in order to ensure sufficient linearity and prevent destructive read [2]. The shortest pulse width needs to be  $<250$ ps while driving a large RC  $WL$ , which is challenging due to the row pitch-matching constraints. Hence, sub-ranged read is proposed where 4 MSBs and 4 LSBs are stored in adjacent columns (column pair), and read simultaneously on  $BL_{MSB}$  and  $BL_{LSB}$ . Then, the charge on  $BL_{MSB}$  is shared with 1/16 of  $BL_{LSB}$  charge via switches  $\emptyset_{con}$  and  $\emptyset_{merge}$ . Capacitors attached to  $BL$ s enable fine-tuning of the 1/16 capacitance ratio. The sub-ranged  $MR-FR$  (Fig. 3) achieves a maximum INL = 0.03 LSB.

In the  $MD$  mode, the  $MR-FR$  enables D-to-A conversion, and replica cell read performs word-level add/subtract by reading  $P$  ( $\bar{P}$  for subtract) from the replica bit-cell array simultaneously with  $D$  (Fig. 3) [2]. The replica bit-cell array stores streamed data  $P$  and can be written directly by  $write BL$  ( $WBL$ )

reducing energy and latency overheads.

The *BLP* (Fig. 4) can be reconfigured to operate in either the *DP* or the *MD* mode for dot product or absolute computation, respectively. In the *MD* mode, an analog comparator and a mux is used to obtain the absolute value, and the multiplier circuit is reconfigured as a *BL*-wise sampler. In the *DP* mode, the comparator is bypassed and *BLB* is chosen by the mux. The mixed-signal capacitive multiplier [4] uses identical bit capacitors to meet the column pitch constraints necessitating sequential processing of multiplicand bits ( $p_i$ ) and thereby limiting the throughput. Sub-ranged multiplication alleviates this problem by employing two 4-b MSB/LSB multipliers operating in parallel. The *BLP* outputs are charge-shared in the *CBLP* and sampled and later converted into a digital value by the ADC. In the *CBLP*, the MSB and LSB rails are charge-shared by first opening  $\emptyset_{con\_rail}$  and then closing  $\emptyset_{merge\_rail}$  to obtain the final output as a weighted sum. The measured accuracy of *BLP* and *CBLP* (including *MR-FR*) (Fig. 4) shows that the maximum error magnitude in the *DP* (*MD*) mode is 5.8% (8.6%) of output dynamic range.

The proposed architecture requires 16X fewer read accesses (and precharges) as compared to the conventional architecture for a fixed volume of data, resulting in up to 5.8X throughput enhancement. This is because *MR-FR* and *BLP* process data in massively parallel manner (128 8-b words per precharge) whereas the normal SRAM mode fetches only 8 8-b words through 4:1 column muxing. Smaller  $\Delta V_{BL}$  and fewer read access reduces data access energy. Charge redistribution-based low-swing computation adds to the energy savings.

Fig. 5 (left) indicates that CORE energy and decision accuracy trade-off with  $\Delta V_{BL}$ . For binary (64-class) decisions,  $\Delta V_{BL} > 15$  mV ( $> 25$ mV) results in  $> 90\%$  detection accuracy, and the CORE energy reduces by 0.2pJ (0.4pJ) per 20mV reduction in  $\Delta V_{BL}$ . Energy breakdown in Fig. 5 (right) indicates that

much of the savings is due to *MR-FR*. The CTRL energy will be amortized in a multi-bank scenario. The measured energy in *DP (MD)* mode is  $5.6\times$  ( $3.7\times$ ) smaller than conventional architecture, with savings up to  $9.7\times$  ( $5.4\times$ ) in a multi-bank scenario.

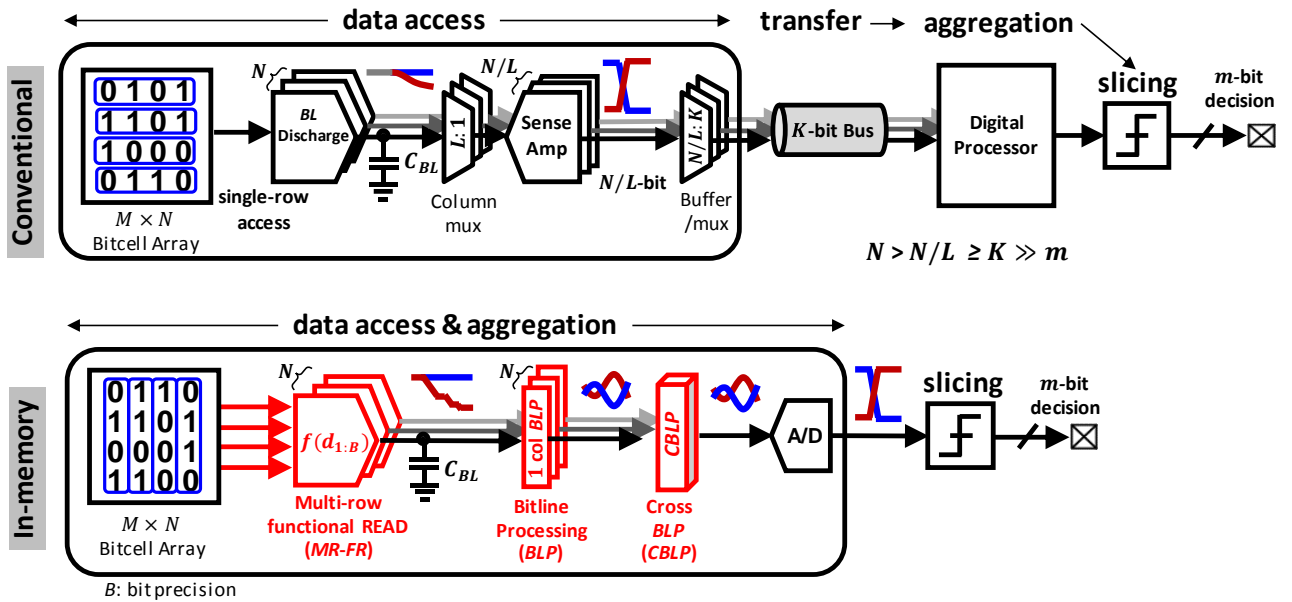
The multifunctional IC (Fig. 6) implements four different algorithms with 2, 4, and 64-class decisions in a  $512\times 256$  SRAM array achieving better decision accuracy and comparable EDP (scaled for 65nm) than single function ICs [1,3]. The chip micrograph (Fig. 7) shows that the deep in-memory circuitry incurs an area overhead of 25% not counting the CTRL.

### **Acknowledgement**

This work was supported by Systems on Nanoscale Information fabriCs (SONIC), one of the six SRC STARnet Centers, sponsored by SRC and DARPA.

### **References**

- [1] H. Kaul, et al., "A 21.5M-Query-Vectors/s 3.37nJ/Vector Reconfigurable k-Nearest-Neighbor Accelerator with Adaptive Precision in 14nm Tri-Gate CMOS," *ISSCC Dig. Tech. Papers*, pp. 260-261, 2016.
- [2] M. Kang, et al., "An Energy-efficient VLSI Architecture for Pattern Recognition via Deep Embedding of Computation in SRAM," *ICASSP*, pp. 8326-8330, 2014.
- [3] J. Zhang, et al., "A Machine-learning Classifier Implemented in a Standard 6T SRAM Array," *Dig. Symp. VLSI Circuits*, June 2016.
- [4] M. Kang, et al., "An Energy-efficient Memory-based High-throughput VLSI Architecture for Convolutional Networks," *ICASSP*, pp. 1037-1041, 2015.



#### Multi-functions in each stage

Stage	Configurations		
<b>Multi-row Functional READ (MR-FR)</b>	① Normal READ	② Digital to Analog conv.	③ ADD /SUBT
<b>BLP</b>	Reconfigurable MULT		③ COMP /ABS
	① MULT	② BL Sample	
<b>CBLP</b>	① Sub-ranging		② ADD
<b>slicing</b>	① MIN/MAX		② Linear Combination

#### Configurations of each stage for 4 algorithms

mode	4 algorithms	MR-FR	BLP	CBLP	slicing
<b>Dot Product (DP) mode</b> ( $\sum D_i P_i$ )	Support Vector Machine (SVM)	②	①, ②	①, ②	②
	Matched Filter (MF)	②	①, ②	①, ②	②
<b>Manhattan Distance (MD) mode</b> ( $\sum  D_i - P_i $ )	K-nearest Neighbor (KNN)	②, ③	②, ③	②	External process
	Template Matching (TM)	②, ③	②, ③	②	①

Figure 1: Conventional and proposed multi-functional deep in-memory architecture for inference applications.

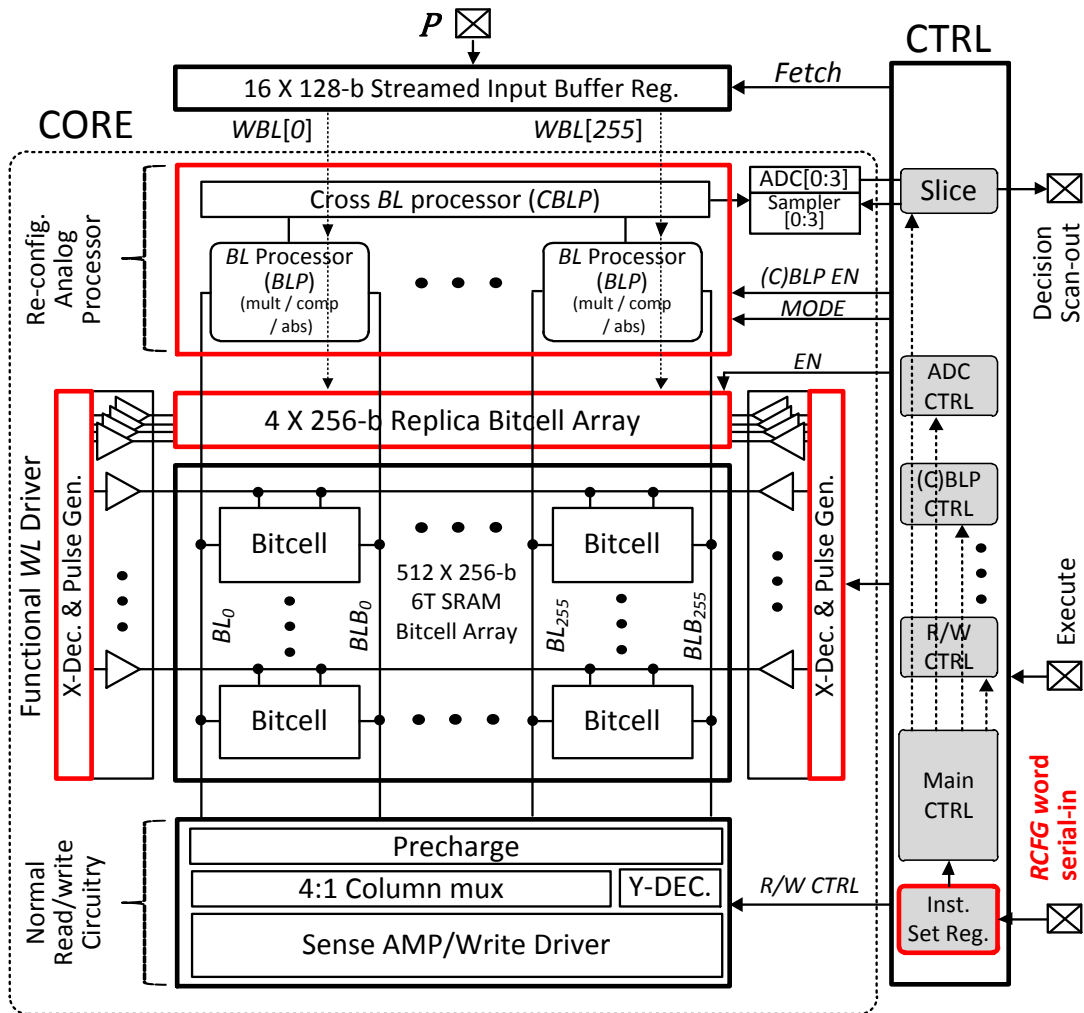


Figure 2: Deep in-memory processor architecture.

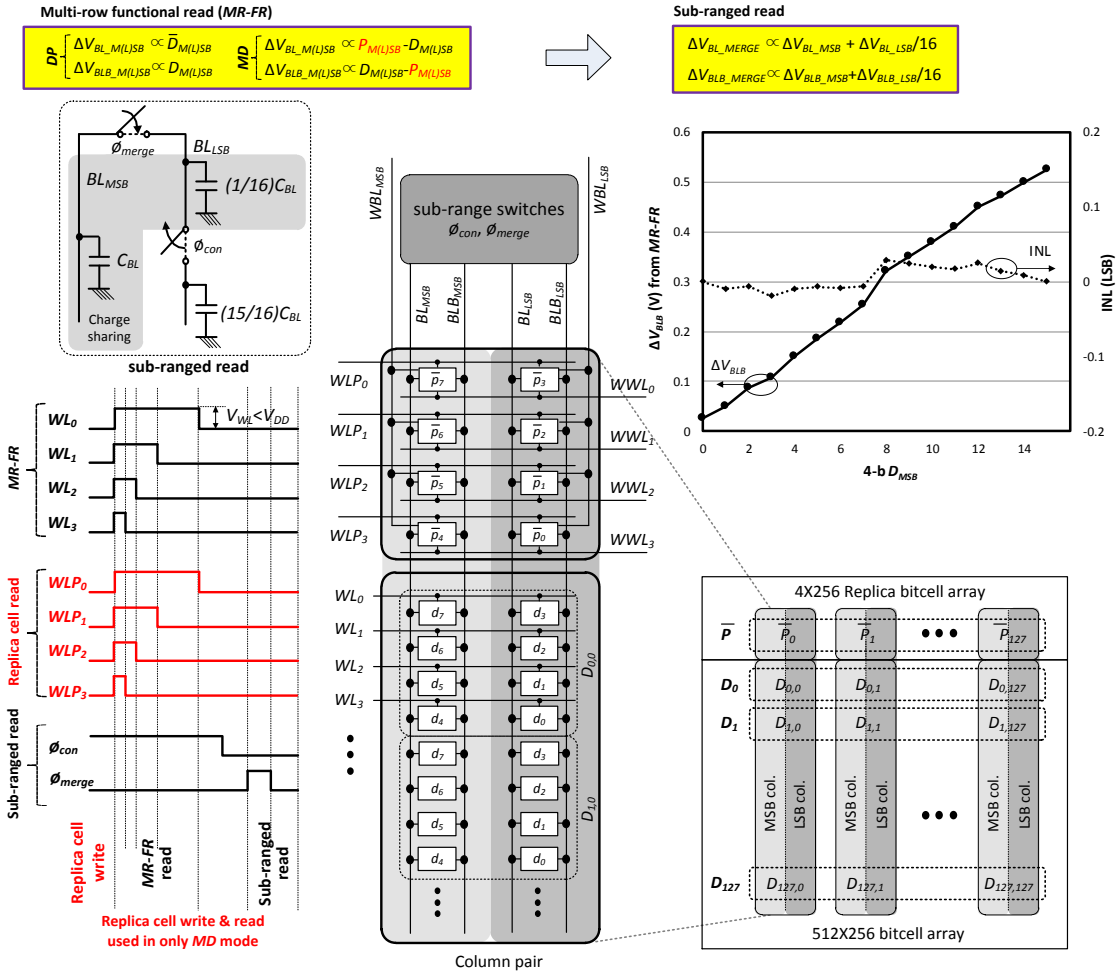


Figure 3: Sub-ranged multi-row functional read (MR-FR) and measured accuracy.



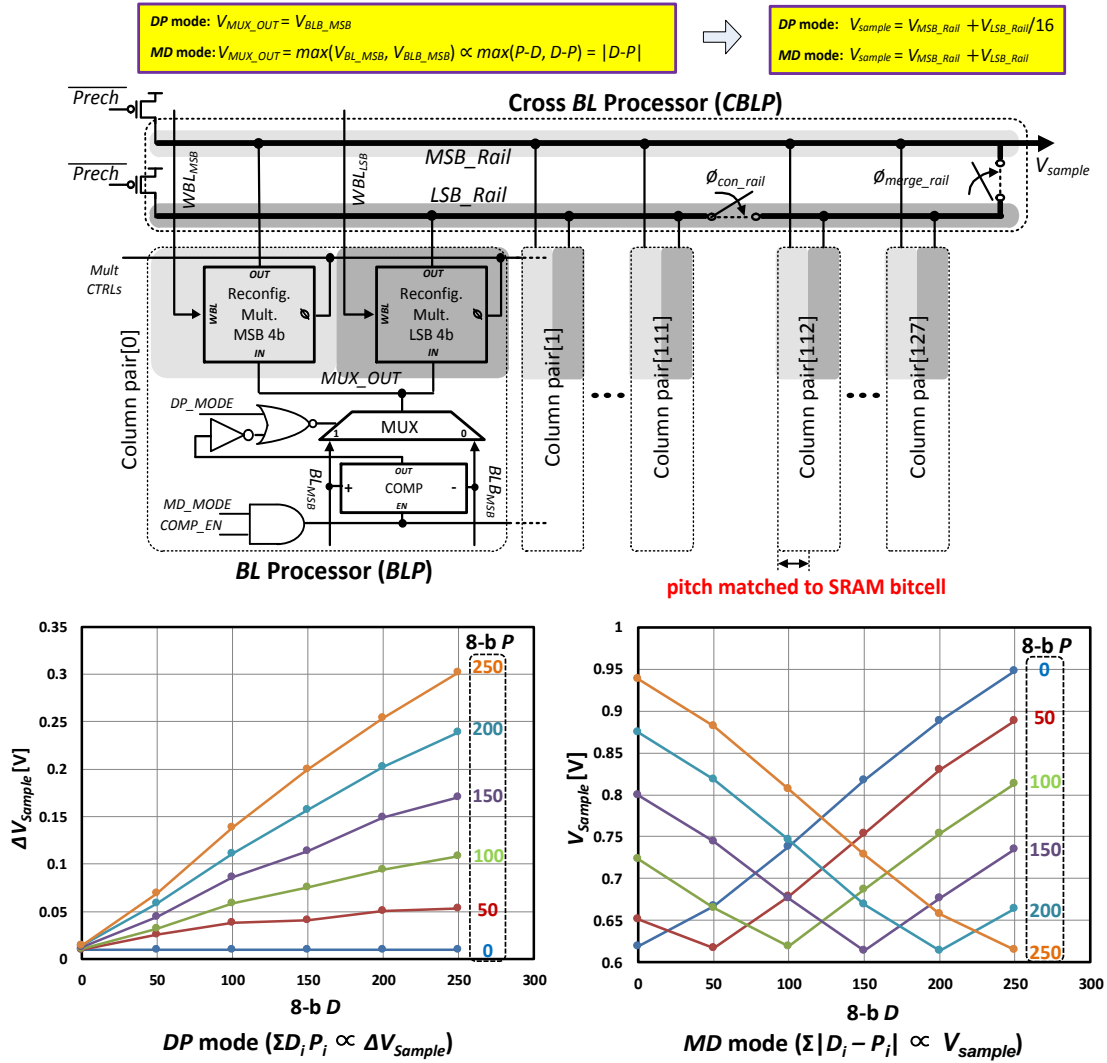


Figure 4: Pitch-matched BL processing (BLP), cross BL processing (CBLP), and measured accuracy (@  $D_0 = D_1 = \dots = D_{255}, P_0 = P_1 = \dots = P_{255}$ ).

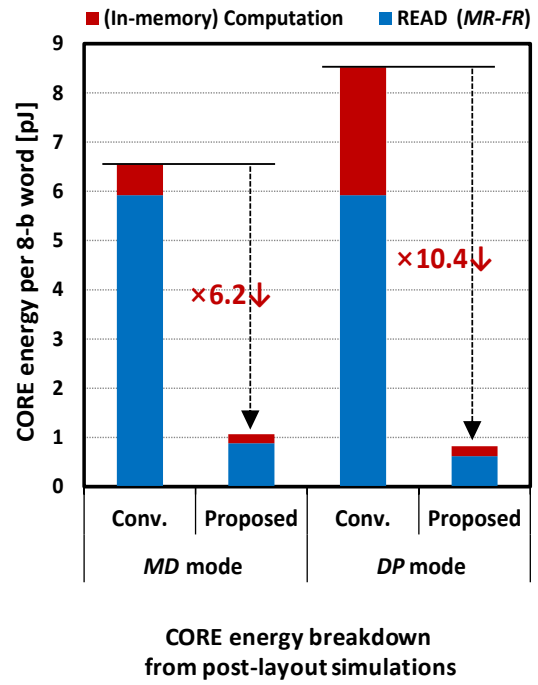
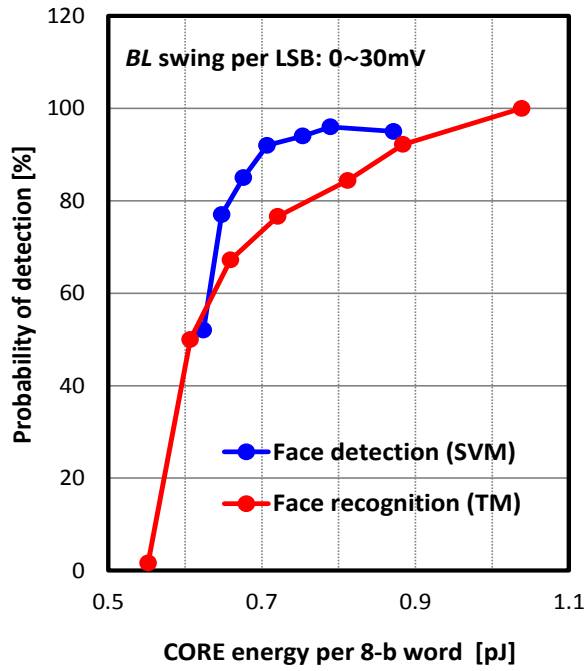


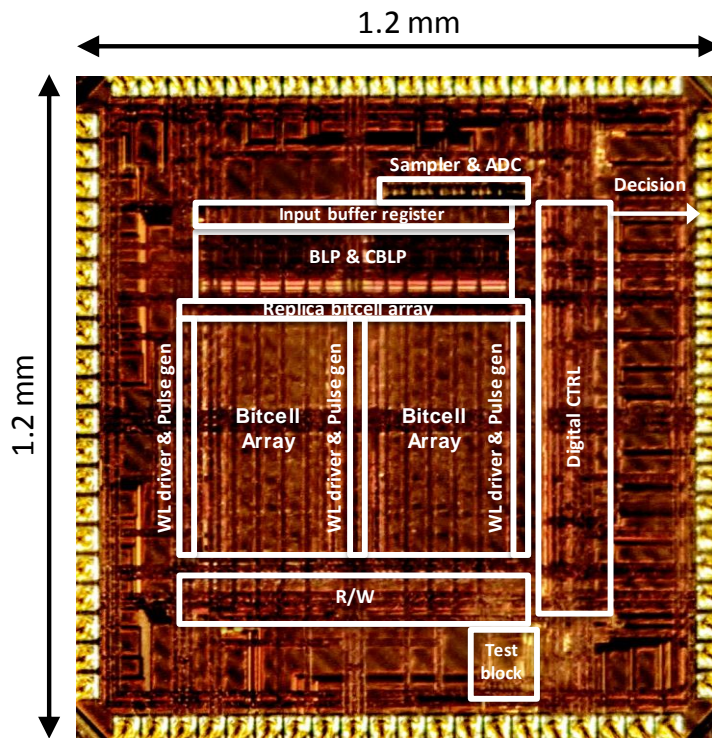
Figure 5: Measured energy vs. detection accuracy trade-offs, and CORE energy breakdown.

	Application	Algorithm	Dataset ( <i>P</i> : Query input, <i>D</i> : data stored in array)
1	Face detection (binary class)	Support Vector Machine ( <i>SVM</i> )	MIT CBCL dataset <i>P</i> : 23 X 22 8-b pixel image (face / non-face), 100 query inputs tested <i>D</i> : Feature extractor and classifier combined 23 X 22 8-b word coefficient
2	Event (Gun shot) detection (binary class)	Matched filter ( <i>MF</i> )	<i>P1</i> : Gun shot sound contaminated by AWGN with 3 dB SNR or <i>P2</i> : Only AWGN with equal power of "signal + AWGN" in <i>P1</i> total 100 query inputs tested <i>D</i> : gun shot mono sound data with 256 8-b words
3	Face recognition (64 classes)	Template matching with Manhattan distance ( <i>TM</i> )	MIT CBCL dataset, 16 X 16 8-b pixel image for <i>P</i> and <i>D</i> <i>P</i> : one of the 64 candidate faces in <i>D</i> , 64 query inputs tested <i>D</i> : 64 candidate faces
4	Hand-written number recognition (4 classes)	K-nearest neighbor ( <i>KNN</i> )	MNIST dataset, 4 classes from "0" to "3" (due to array size limit) 16 X 16 8-b pixel image for <i>P</i> and <i>D</i> <i>P</i> : image from 4 classes, 100 query inputs tested <i>D</i> : 16 images per class

	Tech. (nm)	# of Algorithms	Memory size	Precision (b)	Decision Throughput (Decisions/s)	Decision Energy (pJ/decision)	Decision EDP (fJ-s)	Accuracy
This work	65 CMOS	4 ( <i>SVM</i> , <i>MF</i> , <i>KNN</i> , <i>TM</i> )	SRAM 512 X 256-b	8x8	<i>SVM</i> : 9.3M	963.1 / 462.4†	0.1 / 0.05†	95 %
					<i>MF</i> : 18.5M	481.5 / 231.2†	0.03 / 0.01†	100 %
					<i>TM</i> : 312.5K	33.6K / 17.5K†	107.3 / 56.0†	100 %
					<i>KNN</i> : 312.5K	33.6K / 17.5K†	107.4 / 56.0†	92 %
8-b digital*	65 CMOS	synthesized dedicated processor per algorithm	SRAM 512 X 256-b	8x8	<i>SVM</i> : 1.7M	4.5K	2.6	96 %
					<i>MF</i> : 3.4M	2.2K	0.6	100 %
					<i>TM</i> : 54.3K	93.0K	1715.3	100 %
					<i>KNN</i> : 54.3K	93.0K	1715.3	90 %
[1]††	14 Tri-gate	1 ( <i>KNN</i> )	128 byte	8x8	21.5M	3.4K	0.2	Not reported
[3]**	130 CMOS	1 (Ada boost)	SRAM 128 X 128-b	5x1	50M	633.4	0.01	90 %

\* memory (digital) energy & delay measured from prototype IC (post-layout simulations); † assumes a 32 bank configuration; †† single function with SRAM memory access cost not included; \*\* single function with 1b weight vector

Figure 6: Application level gains in energy efficiency, delay, accuracy, and comparison with prior arts.



<b>Technology</b>	65 nm CMOS	
<b>Die size</b>	1.2 mm × 1.2 mm	
<b>CTRL operating freq.</b>	1 GHz	
<b>SRAM capacity</b>	16 KB (1 bank of 512 × 256-b)	
<b>Bitcell dimension</b>	2.11 × 0.92 μm <sup>2</sup>	
<b>Supply voltage</b>	CORE: 1.0 V, CTRL: 0.85 V	
<b>Energy per decision (pJ)</b>	<i>SVM</i>	963.1
	Matched filter	481.5
	<i>KNN</i>	33.6K
	Template matching	33.6K
<b>Decision Throughput (Decisions/s)</b>	<i>SVM</i>	1.7M
	Matched filter	3.4M
	<i>KNN</i>	54.3K
	Template matching	54.3K

Figure 7: Die micrograph and chip summary.